# Simultaneous Extraction of Sulfur and Nitrogen Compounds from Model Diesel Fuel Using Neoteric Green Solvents

Hurun E. Suhaimi, Hanee F. Hizaddin,* Irfan Wazeer, Lahssen El Blidi, Mohd A. Hashim, and Mohamed K. Hadj-Kali*

Read Online

ACCESS | Metrics & More | Article Recommendations | Supporting Information

**ABSTRACT:** Removal of nitrogen and sulfur compounds from diesel fuel is essential to comply with the increasing stringent regulations. The extraction capability of two deep eutectic solvents, namely, tetrabutylphosphoniumbromide/ethylene glycol, TBPBr/EG, with molar ratio 1:2, and tetrabutylammoniumbromide/ethylene glycol, TBABr/EG, with molar ratio 1:2, in simultaneously extracting basic nitrogen, nonbasic nitrogen, and sulfur compounds represented by pyridine, indoline, and dibenzothiophene (DBT) from $n$-hexadecane, was investigated. Two pseudo-ternary phase diagrams of (TBPBr/EG + (pyridine + indoline + DBT) + $n$-hexadecane) and (TBABr/EG + (pyridine + indoline + DBT) + $n$-hexadecane) were predicted via a conductor-like screening model for real solvents (COSMO-RS) and experimentally validated at 298.15 K and 1 atm. Both solvents showed zero cross-contamination, indicating the suitability of all solvents as extraction solvents. The tie lines obtained for both COSMO-RS and experiments were in agreement and had root-mean-square deviation (RMSD) values of less than 5% for both systems. Selectivity and distribution ratio calculated indicates the suitability of both solvents in extracting sulfur and nitrogen compounds from hexadecane. Two new parameters, namely, extraction efficiency, $\alpha$, and extraction affinity, $\beta$, were introduced to ease the performance comparison of both solvents. TBPBr/EG shows a slightly better performance than TBABr/EG. Other than that, the presence of multiple solutes shows low effects on the performance of these solvents.
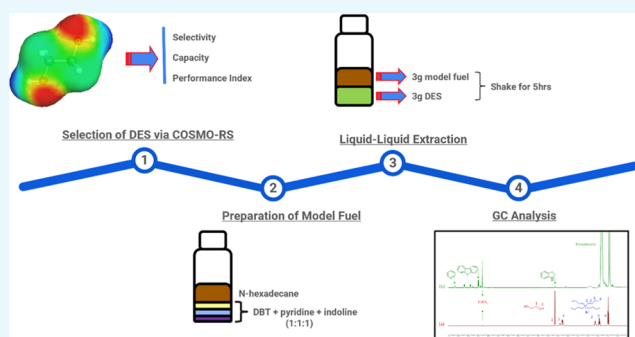
## 1. INTRODUCTION

Sulfur and nitrogen compounds are naturally found in crude oil where they are more abundant in the heavier oil.[1] The refining industry pays a lot of attention to separating these compounds from crude oil due to their adverse effects on the quality of the refined products and the negative impact on the environment, economy, and ecosystem.[2] The presence of nitrogen compounds in crude oil reduces the efficiency of the hydrodesulfurization (HDS) process via competitive adsorption of the catalyst. In addition, it also reduces the stability of the fuels, making it a challenge for safe storage and transportation.[3] The incomplete removal of sulfur and nitrogen compounds causes emission of $SO_x$ and $NO_x$ gases from the fuel combustion and affects the air quality and human health.[4] In recent years, stringent regulations on the permissible levels of sulfur and nitrogen compounds in transportation fuels have been enforced. The United States has limited the permissible nitrogen content in diesel to less than 1 ppm in 2010, whereas the limit for sulfur content has been decreased to an ultralow level (i.e., less than 15 ppm) in many countries including the United States, Japan, the European Union since 2006, and in China since 2016.[4−8]

Currently, the conventional process to remove sulfur and nitrogen compounds from diesel is hydrotreatment, specifically, hydrodesulfurization (HDS) and hydrodenitrogenation (HDN) processes. These conventional hydrotreating processes occur at high pressure and temperature.[4,9−11] Apart from that, the need for high volumes of hydrogen gas and a large amount of catalyst contribute to the high operating cost of the hydrotreatment process.[5] The need to further remove sulfur and nitrogen compounds to ultralow levels requires more severe operating conditions and is putting a strain on the refining industry.[12]

Several alternative separation processes have been reported in the literature to replace the hydrotreatment process, such as adsorptive desulfurization, oxidative desulfurization, and biological desulfurization.[10,11,13−15] Solvent extraction technique is an attractive process as it has benign operating conditions
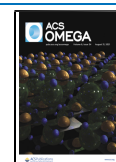
**Table 1. Previous Studies on Simultaneous Extraction of Sulfur and Nitrogen Compounds from Fuel**

| solvent/catalyst | hydrocarbon | sulfur and nitrogen compounds | reference |
|---|---|---|---|
| TBPBr/sulfolane (1:4) | *n*-heptane/simulated gasoline/ simulated diesel | thiophene, DBT, pyridine, carbazole | 5 |
| MTPPBr/AceA (1:4) | *n*-decane | thiophene, quinoline, pyyrole | 23 |
| ChCl/EG (1:2) | 26% of *n*-hexane | 6% of thiophene | 24 |
| ChCl/EG (1:3) | 26% of *n*-heptane, 26% of *i*-octane | 6% of pyridine | |
| ChCl/EG (1:3.5) | 10% of toluene | | |
| catalyst: tungsten/zirconia + $H_2O_2$ | hydrotreated diesel, hydrotreated straight run gas oil | DBT, BT, thiophene, 4-MDBT, 4,6-DMDBT | 14 |
| catalyst: vanadium-substituted Dawson-type polyoxometalate anchored on silica gel + $H_2O_2$ + acetonitrile | simulated diesel, real diesel | DBT, BT, 4,6-DMDBT, quinoline | 25 |

because it can be operated at moderate temperature and pressure.[11,14,15] However, one of the major challenges in using this technique is to select the ideal solvents that would have high selectivity and capacity toward both sulfur and nitrogen compounds.[7] Conventional organic solvents used in most extractive separation processes generally have high vapor pressure and cause cross-contamination between the extract and raffinate phases, thus making it a challenge for solvent regeneration and product recovery. Ionic liquids (ILs) and deep eutectic solvents (DESs) have emerged as alternative solvents to replace conventional organic solvents. This is largely due to their high thermal stability and negligible vapor pressure.[4,7] These solvents are also known as "designer solvents" since they can be tailored to suit the desired applications by manipulating the cation and anion combination for the salt of the ILs or to manipulate the molar ratio of the salt and hydrogen-bond donor (HBD) for DESs. However, although ILs and DESs in general share similar physical properties, DESs have the advantage in its simplicity of the synthesis process compared to ILs.[16] The preparation of DES may take a simple physical mixing of a quaternary salt and HBD at a certain molar ratio until a clear, homogenous liquid is formed. This liquid is a eutectic mixture formed through a hydrogen bonding between salt and HBD, where its freezing point is much lower than its individual freezing point.[17] The steps to synthesize ILs, on the other hand, involve more complex processes.[18]

Nonetheless, ILs and DESs have been explored in many fields of applications such as separation of aromatic hydrocarbons from naphtha, electrochemistry, and nanomaterial.[19,20] In fact, Gao et al. used ILs in an oxidative desulfurization process to extract sulfur compounds from fluidized catalytic cracking (FCC) fuel oil where ILs were used as both extractants and catalysts.[21] They managed to reduce the sulfur content in the diesel to meet the specification of ultralow sulfur diesel from 150 to 8.1 ppm. In a different study, Laredo et al. tested the ability of their synthesized IL to extract various nitrogen compounds from gas feed oil.[22] It was found that neutral nitrogen compounds, i.e., carbazole-derived compounds, were more easily extracted compared to basic nitrogen compounds, i.e., pyridinic compounds. The study also reported that the presence of sulfur compounds in the fuel oil did not affect the extracting ability of the IL toward nitrogen compounds. Table S1, provided in the Supporting Information, contains the list of work done on the extraction of single extraction of sulfur or nitrogen compound from fuel oil. Nevertheless, there is a lack of study on the application of DESs in extracting sulfur and nitrogen compounds simultaneously. To date, only a few publications have reported on the

simultaneous extraction of nitrogen and sulfur using ILs and DESs, as presented in Table 1.

Due to the huge number of possibly existing DES from various permutations of cation, anion, HBD choice, and the salt/HBD molar ratio, it is challenging to select the most appropriate combinations to synthesize effective DESs for our application of interest, which is simultaneous denitrogenation and desulfurization of liquid fuels. Additionally, there is limited data on the physical properties of the DESs and the thermodynamic behavior of liquid mixtures containing DESs available in the literature unlike the conventional organic solvents. The use of the group contribution method (GCM) such as UNIFAC has been widely reported to approximate the activity coefficient and thermophysical properties of solvents.[26] However, due to the complexity of the calculation and lack of experimental data on DES, this method proves to be challenging. Therefore, a method that does not rely on experimental data to predict the thermodynamic behaviors of liquid mixtures is more favorable. This can be achieved using the conductor-like screening model for real solvents (COSMO-RS). Using COSMO-RS, the infinite dilution activity coefficient ($\gamma^\infty$) of solutes in solvents can be estimated. This enables the quantification of DES performance in extracting trace amounts of solute from liquid mixtures.[16]

COSMO-RS uses the continuum solvation model where a virtual conductor is created to surround the molecule. A quantum calculation is then performed, producing a screening charge density known as $\sigma$, which is converted to a function of surface composition known as the $\sigma$-profile.[27] This file, known as the. *cosmo* file, is used for computing the molecular energy by considering interactions such as van der Waals (vdW), electrostatic, and hydrogen bonding.[26] The computed $\sigma$-profile and $\sigma$-potential ($\mu(\sigma)$) aid in describing the molecular interaction between mixtures in terms of polarity and affinity.[16]

The most popular application of COSMO-RS for liquid mixture separation is the prediction of phase equilibria. Naik et al. used COSMO-RS in predicting the behavior of methyltriphenylphosphonium bromide—ethylene glycol with a 1:4 molar ratio.[28] Warrag et al. used COSMO-RS to predict the interaction of tetraethylammonium chloride—ethylene glycol (1:2), tetraethylammonium chloride—glycerol (1:2), methyltriphenylammonium bromide—ethylene glycol (1:3), and metyltriphenylphosphonium bromide—glycerol (1:3) with thiophene.[29] Gouveia et al. predict the ternary line of three DESs, namely, cholinium chloride—levulinic acid, benzylcholinium chloride—levulinic acid, and tetrabutylammonium chloride—levulinic acid at a molar ratio of 1:2, where all of them show close agreement to the experimental values.[30] Hizaddin et al. calculated a 2.51% root-mean-square deviation (RMSD) value between the experimental tie line and the

predicted tie line by COSMO-RS for tetrabutylphosphonium bromide−ethylene glycol (1:2) and tetrabutylammoniumbromide−ethylene glycol (1:2).[31]

Apart from that, COSMO-RS is also used to predict thermodynamic properties and solubility data. Indeed, Hernandez-Bravo et al. determined the solubility of asphaltene in IL, whereas Warrag et al. managed to confirm the solubility of thiophene in tetraethylammonium chloride−ethylene glycol (1:2), tetraethylammonium chloride−glycerol (1:2), methyltriphenylammonium bromide−ethylene glycol (1:3), and metyltriphenylphosphonium bromide−glycerol (1:3) DESs using COSMO-RS.[29,32]

Estimation of the activity coefficient was also done in an effort to predict the best extracting solvent. Further calculation of selectivity and the distribution coefficient helps in narrowing down the choice of the solvent based on the preliminary screening results. This was explored by Hizaddin et al., where 94 DESs were screened for their performance evaluation in extractive denitrogenation using the predicted $\gamma^\infty$.[16] Further calculation of selectivity, capacity, and performance index was performed to choose the solvent with the highest performance. Gouveia et al. also successfully predicted the selectivity and distribution ratio of cholinium chloride−levulinic acid, benzylcholinium chloride−levulinic acid, and tetrabutylammonium chloride−levulinic acid with the molar ratio of 1:2.[30] Additionally, the use of COSMO-RS has been extended to be of use in the conceptual design of extraction equipment. The COSMO-RS-based model was used in ASPEN HYSYS and ASPEN Plus in the separation of aromatic and aliphatic using IL, separation of aromatic and aliphatic from naphtha using IL, extraction of aromatic compound from pyrolysis gasoline using IL, and production of ultralow sulfur diesel.[4,25,33−35]

In this work, COSMO-RS was used to screen DESs for the simultaneous extraction of nitrogen and sulfur compounds from diesel fuel and in elucidating the interaction between the solvents and solutes. Table S2 in the Supporting Information reports the list of screened DESs used in the COSMO-RS preliminary study. Selected DESs were then used for experimental validation to compare their performance in the simultaneous extraction of sulfur and nitrogen compounds. The selected DESs used in this work are tetrabutylphosphonium bromide−ethylene glycol, TBPBr/EG (1:2), and tetrabutylammoniumbromide−ethylene glycol, TBABr/EG (1:2). In this study, we focused our interest on two main points: (i) the capability of these solvents to simultaneously extract nitrogen and sulfur compounds and (ii) the effects of the presence of sulfur compounds on solvent capability in extracting nitrogen compounds.

## 2. RESULTS AND DISCUSSION

**2.1. COSMO-RS Screening.** Screening of 44 DESs was done, and the lists of selectivity ($S^\infty$) and capacity ($C^\infty$) at infinite dilution (individual and average) were calculated using eqs 1 and 2. $S^\infty$ and $C^\infty$ quantitatively describe the affinity of DES toward the solute and estimation on the amount of DESs needed during the extraction, respectively. Values higher than unity for both parameters indicate good $S^\infty$ and $C^\infty$ of the solvent.

$$S^\infty = \frac{\gamma^\infty_{SU}}{\gamma^\infty_H} \qquad (1)$$

$$C^\infty = \frac{1}{\gamma^\infty_H} \qquad (2)$$

where $S^\infty$ is selectivity at infinite dilution, $C^\infty$ is capacity at infinite dilution, $\gamma^\infty_{SU}$ is the activity coefficient of the solute at infinite dilution, and $\gamma^\infty_H$ is the activity coefficient of hexadecane at infinite dilution.

Due to the huge difference in the value of individual $S^\infty$ and $C^\infty$, graphs of ln $S^\infty$ and ln $C^\infty$ against DESs were plotted. As can be seen in Table 2 and Figure 1, choline-based DES possessed the highest selectivity with pyridine > indoline > dibenzothiophene (DBT). From Figure 1, we can also see that tetramethyl-based, tetrabutyl-based, and triphenyl-based DESs have similar trend values. This high $S^\infty$ value of choline-based DES toward pyridine shows a highly selective property of this DES type toward pyridine. This behavior might be caused by the structures of both choline and pyridine themselves. The choline ion has one oxygen atom on top of the nitrogen atom, whereas the other cation only has either a nitrogen or a phosphorus atom. This gives choline extra electronegativity, where it contributes to hydrogen-binding formation. The list of cations used can be found in Table S3.

Other than that, the simple structure of pyridine compared to indoline and dibenzothiophene might also contribute to this factor. Due to this huge difference in the individual $S^\infty$, an average of $S^\infty$ was calculated to ease the comparison of $S^\infty$ of each DES. This is illustrated in Figure 2, where a clearer comparison of $S^\infty$ can be made between the DESs. Choline-based DESs take precedent over other types of DESs, with ChCl/MA (1:2) and ClChCl/U (1:2) having the highest $S^\infty$. Then, it is followed by triphenyl-based, tetrabutyl-based, and tetramethyl-based DESs. The extraordinarily high values of selectivity and capacity at infinite dilution reported by ChCl/MA DESs at 1:1 and 1:2 molar ratio are consistent with our previous publication on DES screening for denitrogenation of the model diesel fuel, where it has been explained that the performance of the DES may have been attributed to the presence of two −COOH groups in its dicarboxylic acid functional group, which helps enhance the hydrogen-bonding interaction with aromatic compounds and facilitates the extraction of sulfur and nitrogen compounds.[16] The same reference has also discussed why DES with a chlorocholine cation (ClChCl/U (1:2)), i.e., a chlorocholine-based DES, is expected to show a high value of $S^\infty$ due to the presence of the Cl atom that is attached to the choline cation, and this increases the polarity of the DES and makes it more selective toward the aromatic nitrogen and sulfur compounds compared to the diesel compounds.

Figures 3 and 4 illustrate the $C^\infty$ trend value for all 44 DESs. This $C^\infty$ value defines qualitatively the amount of DES needed during the extraction process. This is important as it is directly related to the operating cost involved in the extraction process. As can be seen in Figure 3, a more distributed value of $C$ can be seen for all three solutes. All DESs have a higher $C^\infty$ value for pyridine compared to the other two solutes. Choline-based DESs have a lower value of $C^\infty$ compared to the other three types of DESs, except for ChCl/MA (1:2). This shows that the values of and $C^\infty$ and $S^\infty$ are reciprocal to each other. Due to this, another parameter will be used for evaluating these DESs, which is the performance index, PI. PI, as shown in eq 3, is the product of $S^\infty$ and $C^\infty$, and it calculates the overall performance of solvents. This parameter is useful if the values of $S^\infty$ and $C^\infty$ are similar.

**Table 2. List of Performance Index (PI), Selectivity ($S^\infty$), and Capacity ($C^\infty$) of DESs at Infinite Dilution Screened via COSMO-RS**

| DES | selectivity | | | | capacity | | | | performance index | | | |
|---|---|---|---|---|---|---|---|---|---|---|---|---|
| | pyridine | indoline | DBT | average | pyridine | indoline | DBT | average | pyridine | indoline | DBT | average |
| TMACl/G (1:2) | 8555.2 | 4708.4 | 459.9 | 4574.5 | 1.38 | 0.76 | 0.07 | 0.74 | 11 769.9 | 3565.0 | 34.0 | 5123.0 |
| TMACl/EG (1:2) | 14 872.1 | 7005.3 | 749.0 | 7542.1 | 1.35 | 0.64 | 0.07 | 0.69 | 20 121.4 | 4464.4 | 51.0 | 8212.3 |
| TMACl/PAA (1:2) | 3421.2 | 1794.7 | 477.8 | 1897.9 | 4.88 | 2.56 | 0.68 | 2.71 | 16 690.1 | 4593.1 | 325.6 | 7202.9 |
| TBACl/MA (1:2) | 5557.0 | 992.9 | 163.9 | 2237.9 | 10.69 | 1.91 | 0.32 | 4.31 | 59 425.0 | 1897.0 | 51.7 | 20 457.9 |
| TBACl/G (1:2) | 432.7 | 355.4 | 48.1 | 278.7 | 2.27 | 1.86 | 0.25 | 1.46 | 981.7 | 662.3 | 12.1 | 552.1 |
| TBACl/TEG (1:2) | 148.8 | 113.1 | 22.4 | 94.8 | 4.52 | 3.43 | 0.68 | 2.88 | 671.7 | 388.4 | 15.3 | 358.5 |
| TBACl/EG (1:2) | 335.3 | 265.5 | 41.4 | 214.0 | 2.37 | 1.88 | 0.29 | 1.51 | 795.6 | 498.7 | 12.1 | 435.5 |
| TBACl/PAA (1:2) | 144.0 | 127.4 | 43.3 | 104.9 | 5.73 | 5.07 | 1.72 | 4.17 | 824.9 | 645.7 | 74.5 | 515.0 |
| TBACl/CapA (1:2) | 22.0 | 29.7 | 7.8 | 19.8 | 4.18 | 5.64 | 1.48 | 3.77 | 92.0 | 167.6 | 11.6 | 90.4 |
| TBACl/AceA (1:2) | 120.4 | 147.9 | 39.1 | 102.4 | 4.13 | 5.07 | 1.34 | 3.51 | 496.9 | 750.1 | 52.3 | 433.1 |
| TBPBr/EG (1:2) | 508.0 | 318.0 | 51.9 | 292.6 | 3.15 | 1.97 | 0.32 | 1.81 | 1600.3 | 627.0 | 16.7 | 748.0 |
| TBABr/EG (1:2) | 622.3 | 378.3 | 59.6 | 353.4 | 3.01 | 1.83 | 0.29 | 1.71 | 1875.2 | 693.0 | 17.2 | 861.8 |
| MTPPB/G (1:2) | 3429.0 | 1624.2 | 304.1 | 1785.8 | 3.31 | 1.57 | 0.294 | 1.73 | 11 355.2 | 2547.6 | 89.3 | 4664.0 |
| MTPPBr/G (1:3) | 4994.9 | 1890.3 | 293.4 | 2392.9 | 4.13 | 1.56 | 0.243 | 1.98 | 20 645.1 | 2956.7 | 89.3 | 7897.0 |
| MTPPBr/G (1:4) | 6422.8 | 2105.5 | 287.8 | 2938.7 | 4.99 | 1.64 | 0.223 | 2.28 | 32 033.9 | 3442.4 | 71.2 | 11 849.2 |
| MTPPBr/EG (1:2) | 4016.4 | 1689.8 | 363.6 | 2023.3 | 3.61 | 1.52 | 0.327 | 1.82 | 14 499.0 | 2566.3 | 118.8 | 5728.1 |
| MTPPBr/EG (1:3) | 6049.3 | 1904.6 | 343.8 | 2765.9 | 4.71 | 1.48 | 0.268 | 2.16 | 28 514.7 | 2826.5 | 92.1 | 10 477.8 |
| MTPPB/EG (1:4) | 7997.7 | 2076.6 | 331.0 | 3468.4 | 5.91 | 1.53 | 0.244 | 2.56 | 47 225.4 | 3183.7 | 80.9 | 16 830.0 |
| MTPPB/EG (1:5) | 9789.9 | 2219.4 | 322.3 | 4110.5 | 7.15 | 1.62 | 0.235 | 3.00 | 69 980.7 | 3596.7 | 75.9 | 24 551.1 |
| MTPPB/TEG (1:3) | 616.4 | 281.5 | 63.5 | 320.4 | 8.40 | 3.84 | 0.865 | 4.37 | 5175.9 | 1079.5 | 55.0 | 2103.5 |
| MTPPB/TEG (1:4) | 631.6 | 256.4 | 54.7 | 314.3 | 11.18 | 4.54 | 0.969 | 5.56 | 7061.7 | 1164.2 | 53.0 | 2759.7 |
| MTPPBr/TEG (1:5) | 645.8 | 242.2 | 49.7 | 312.6 | 14.07 | 5.28 | 1.082 | 6.81 | 9084.7 | 1277.3 | 53.8 | 3471.9 |
| ETPPBr/EG (1:2) | 2734.0 | 1250.5 | 282.3 | 1422.3 | 3.79 | 1.73 | 0.391 | 1.97 | 10 360.9 | 2167.4 | 110.4 | 4212.9 |
| ChCl/U (1:2) | 376 375.4 | 150 369.0 | 17 386.7 | 181 377.0 | 0.80 | 0.32 | 0.04 | 0.38 | 299 077.6 | 47 737.3 | 638.2 | 115 817.7 |
| ChCl/EG (1:2) | 39 408.8 | 12 863.6 | 1226.5 | 17 833.0 | 1.34 | 0.44 | 0.04 | 0.61 | 52 745.0 | 5619.8 | 51.1 | 19 472.0 |
| ChCl/G (1:2) | 17 097.9 | 7442.6 | 622.2 | 8387.6 | 1.26 | 0.55 | 0.05 | 0.62 | 21 491.0 | 4072.1 | 28.5 | 8530.5 |
| ChCl/TFA (1:2) | 148 529.8 | 45 056.8 | 7702.7 | 67 096.4 | 1.39 | 0.42 | 0.07 | 0.63 | 206 844.0 | 19 034.2 | 556.3 | 75 478.2 |
| ChCl/PPA (1:1) | 4183.7 | 2644.2 | 503.8 | 2443.9 | 2.13 | 1.34 | 0.26 | 1.24 | 8890.7 | 3551.5 | 128.9 | 4190.4 |
| ChCl/LA (1:2) | 4151.4 | 2472.5 | 498.3 | 2374.1 | 3.72 | 2.22 | 0.45 | 2.17 | 15 439.4 | 5477.0 | 222.4 | 7046.3 |
| ChCl/X (1:1) | 88 103.4 | 35 874.5 | 1472.3 | 41 816.7 | 1.00 | 0.41 | 0.02 | 0.47 | 87 814.3 | 14 559.7 | 24.5 | 34 132.8 |
| ChCl/DS (1:1) | 12 675.9 | 5639.8 | 409.5 | 6241.7 | 1.17 | 0.52 | 0.04 | 0.57 | 14 792.4 | 2928.2 | 15.4 | 5912.0 |
| ChCl/DIS (1:2) | 35 841.0 | 13 036.8 | 1114.5 | 16 664.1 | 1.87 | 0.68 | 0.06 | 0.87 | 67 124.9 | 8881.1 | 64.9 | 25 357.0 |
| ChCl/MA (1:1) | 349 484.7 | 91 756.5 | 10 306.0 | 150 515.8 | 1.16 | 0.31 | 0.03 | 0.50 | 406 926.4 | 28 050.0 | 353.9 | 145 110.1 |
| ChCl/MA (1:2) | 2 100 543.5 | 184 356.9 | 15 256.7 | 766 719.1 | 5.14 | 0.45 | 0.04 | 1.88 | 10 792 658.5 | 83 135.0 | 569.4 | 3 625 454.3 |
| EChCl/U (1:2) | 252 140.4 | 110 967.4 | 10 487.6 | 124 531.8 | 0.93 | 0.41 | 0.04 | 0.46 | 234 405.2 | 45 401.8 | 405.5 | 93 404.2 |
| AChCl/U (1:2) | 387 282.6 | 169 766.6 | 16 131.3 | 191 060.1 | 0.91 | 0.40 | 0.04 | 0.45 | 351 611.1 | 67 563.3 | 610.0 | 139 928.2 |
| ClChCl/U (1:2) | 1 703 381.6 | 567 730.7 | 53 089.4 | 774 733.9 | 0.64 | 0.21 | 0.02 | 0.29 | 1 091 106.0 | 121 207.0 | 1059.9 | 404 457.6 |
| bhdMEAmCl/U (1:2) | 522 993.5 | 188 426.0 | 16 827.3 | 242 748.9 | 0.92 | 0.33 | 0.03 | 0.43 | 479 010.2 | 62 177.6 | 495.9 | 180 561.2 |
| dEEAmCl/G (1:2) | 9164.7 | 4211.9 | 393.1 | 4589.9 | 1.45 | 0.66 | 0.06 | 0.72 | 13 241.6 | 2796.8 | 24.4 | 5354.3 |
| dEEAmCl/G (1:3) | 12 137.4 | 4659.4 | 399.1 | 5732.0 | 1.93 | 0.74 | 0.06 | 0.91 | 23 382.2 | 3445.9 | 25.3 | 8951.1 |
| dEEAmCl/G (1:4) | 15 549.8 | 4737.7 | 387.6 | 6891.7 | 2.82 | 0.86 | 0.07 | 1.25 | 43 799.4 | 4065.8 | 27.2 | 15 964.1 |
| dEEAmCl/EG (1:2) | 14 668.6 | 5614.9 | 568.6 | 6950.7 | 1.44 | 0.55 | 0.06 | 0.68 | 21 142.0 | 3097.8 | 31.8 | 8090.5 |

**Table 2. continued**

| DES | selectivity | | | | capacity | | | | performance index | | | |
| --- | --- | --- | --- | --- | --- | --- | --- | --- | --- | --- | --- | --- |
| | pyridine | indoline | DBT | average | pyridine | indoline | DBT | average | pyridine | indoline | DBT | average |
| dEEAmCl/EG (1:3) | 21 973.0 | 6012.3 | 560.7 | 9515.3 | 2.21 | 0.60 | 0.06 | 0.96 | 48 475.4 | 3629.3 | 31.6 | 17 378.7 |
| dEEAmCl/EG (1:4) | 26 181.2 | 5873.6 | 524.2 | 10 859.7 | 3.14 | 0.70 | 0.06 | 1.30 | 82 071.5 | 4130.7 | 32.9 | 28 745.0 |
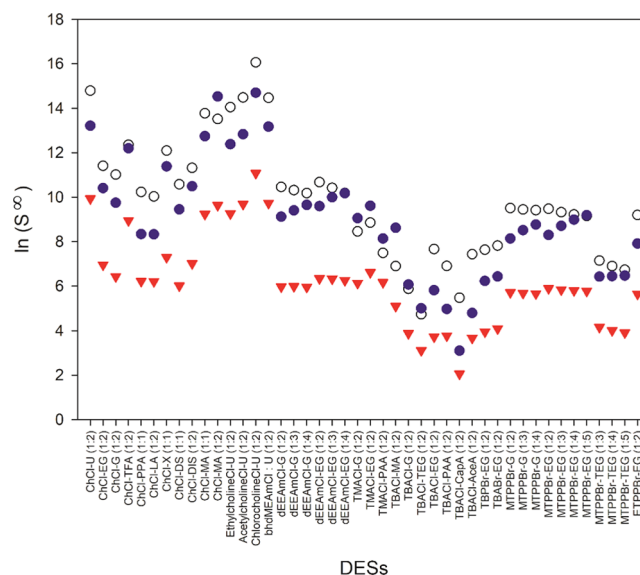


**Figure 1.** $\ln(S^{\infty})$ of DES. Empty circles, indoline; purple circles, pyridine; inverted red triangles, DBT.
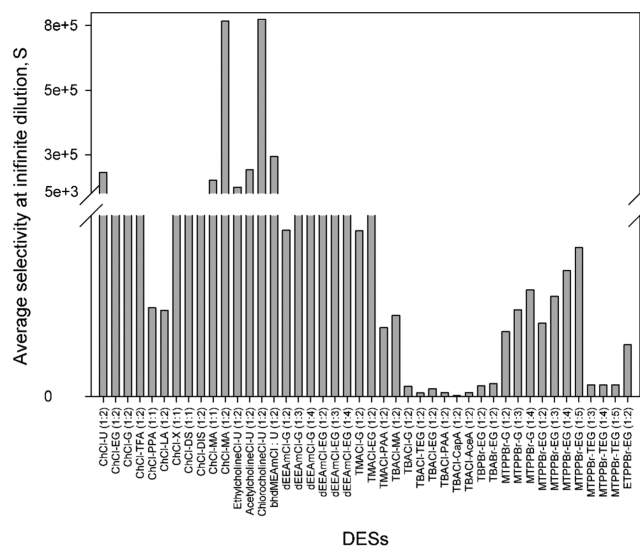


**Figure 2.** Average selectivity, $S$, of DES at infinite dilution.

$$PI = C^{\infty} \times S^{\infty} \tag{3}$$

Figures 5 and 6 show the PI of all DESs with the trend values following the $S^{\infty}$ trend value. The large $S^{\infty}$ directly influences these results, making the PI unsuitable to be used as a benchmarking parameter in selecting DESs for experimental validation. Therefore, the choice of DESs was made based on the average $C^{\infty}$ trend value. This is a fair argument because unlike in the food or pharmaceutical industry where a highly pure product is the main concern, a good balance of $S^{\infty}$ and $C^{\infty}$ values is more important for this work as it will translate to a lower cost. A highly selective DES, i.e., choline-based DES, will require a higher volume, thus leading to a larger cost. Other than that, given the multicomponent nature of our extraction process, it is highly important to ensure that the DES chosen will be able to extract all solutes rather than having selectivity toward one specific solute only.

Ideally, one would choose to use the DES that reports the highest values of selectivity and capacity at infinite dilution to be used in experimental validation. However, other factors also
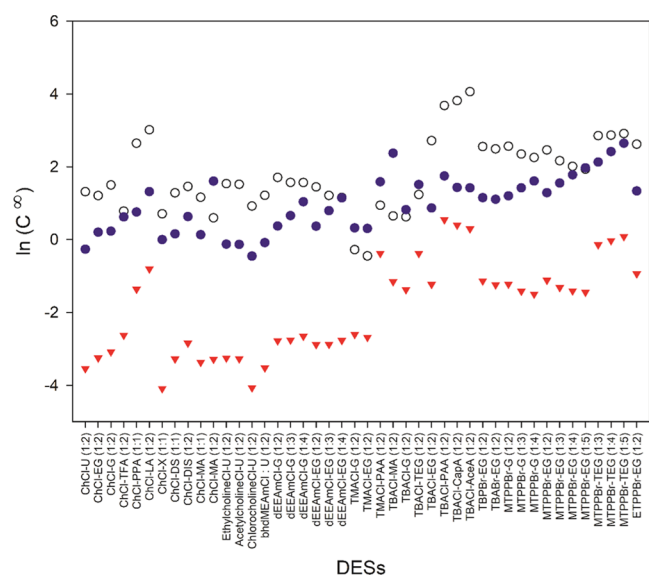
**Figure 3.** ln $C^{\infty}$ of DES. Empty circles, indoline; purple circles, pyridine; inverted red triangles, DBT.
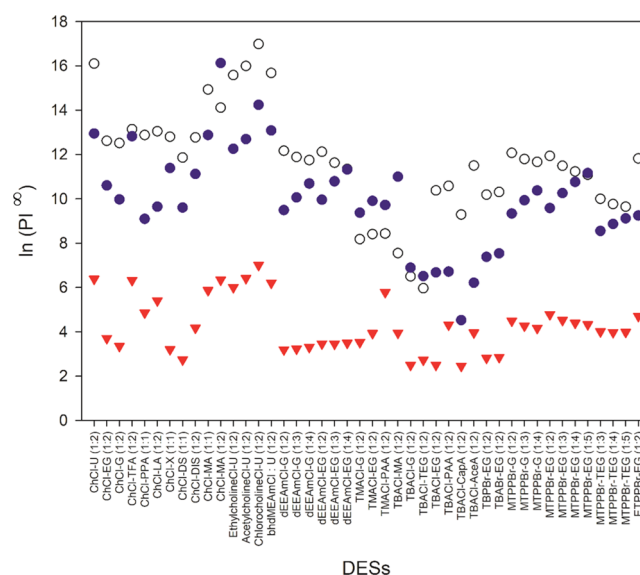


**Figure 5.** ln($PI^{\infty}$) of DES. Empty circles, indoline; purple circles, pyridine; inverted red triangles, DBT.
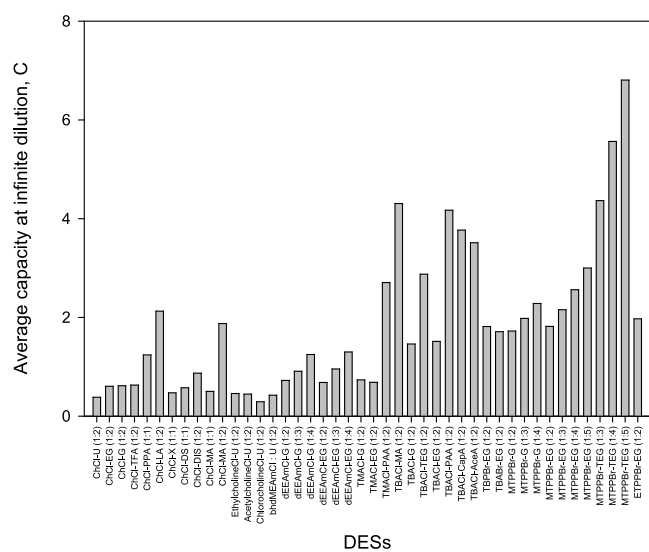


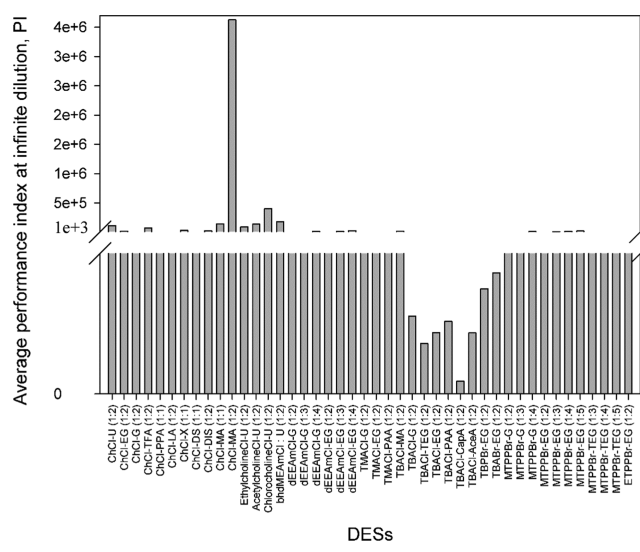**Figure 4.** Average capacity, $C$, of DES at infinite dilution.



**Figure 6.** Average performance index, PI.

contribute to the decision of DESs selected in this work's experimental validation. Apart from a good balance of $S^{\infty}$ and $C^{\infty}$ values, the DESs chosen (TBPBr/EG (1:2) and TBABr/ EG (1:2)) have been used previously in our earlier work to remove heterocyclic nitrogen compounds from the model diesel compound.[31] Thus, in this work, the same DESs were used to remove multiple solutes comprising both nitrogen and sulfur compounds simultaneously, with the same experimental protocol. Both DESs also show reasonable performance in the COSMO-RS screening in this work and are readily available.

**2.2. Elucidating the Molecular Interaction by COSMO-RS.** COSMO-RS can be used for quantitative and qualitative prediction for solvent screening. Quantitative prediction can be performed by predicting the activity coefficient at infinite dilution and estimating the capacity, selectivity, and performance index similar to what was described in Section 2.1. Qualitative screening and elucidation of molecular interaction can also be done by COSMO-RS

through analyzing the generated $\sigma$ profiles and potential of the solute, carrier, and solvent.

Figure 7 presents the $\sigma$-profiles of TBPBr/EG, TBABr/EG, n-hexadecane, pyridine, indoline, and DBT. $\sigma$-Profiles describe the nature of these compounds on their ability to interact with each other. There are two different regions involved in describing the molecular interaction between compounds, which are the hydrogen-bonding and the nonpolar regions. Compounds that possess symmetrical peaks in the nonpolar region have the ability to interact with themselves, thus making it harder to extract or separate them. The vertical lines shown in Figures 7 and 8 are the threshold values of the hydrogen-bond interaction. Any compound that possesses the value of $\sigma$ > +$\sigma_{hb}$ or $\sigma$ < −$\sigma_{hb}$ acts as HBA and HBD, whereas peaks between these values interact via $E_{misfit}$ or $E_{Vdw}$.[36] The $\sigma$ potential describes the affinity of compounds toward each other. A more negative value of $\mu(\sigma)$ is desired as it indicates a higher interaction between components in the mixture. The
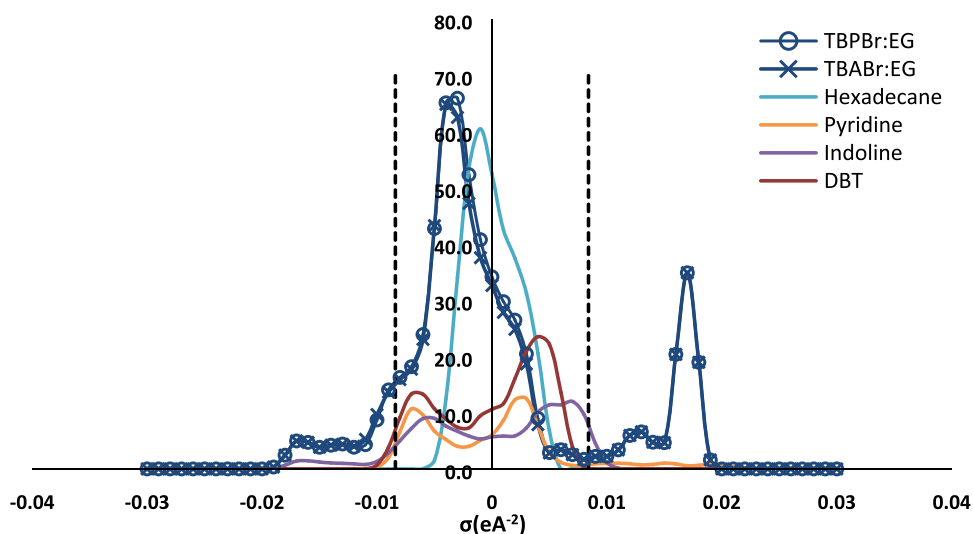
**Figure 7.** $\sigma$ Profiles of TBPBr/EG and TBABr/EG and simulated diesel, with the dashed lines representing the threshold value of the hydrogen-bonding interaction, $\sigma_{hb} = 0.0084$ e A$^{-2}$.
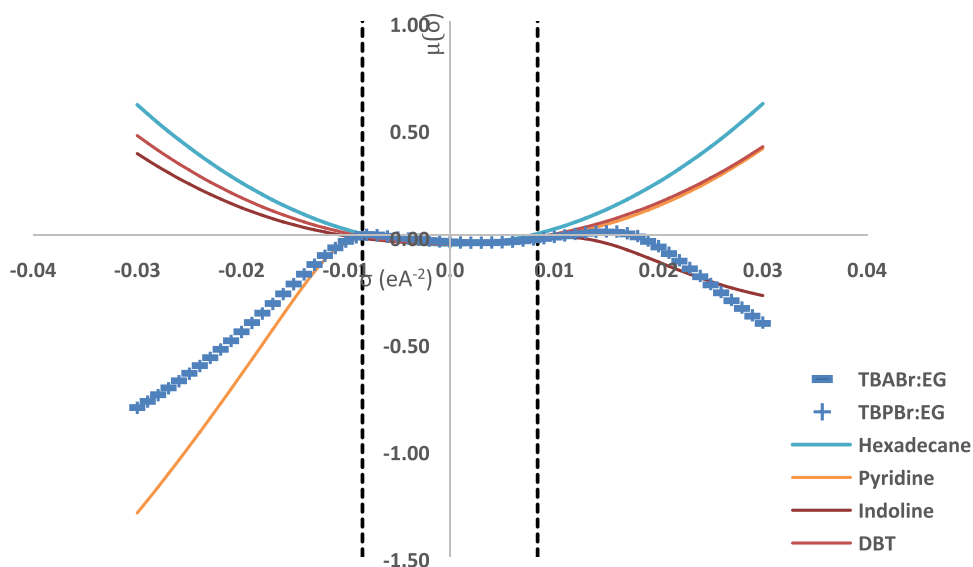


**Figure 8.** $\sigma$ Potentials of TBABr/EG, TBPBr/EG, and simulated diesel. Vertical dashed lines represent the threshold value for the hydrogen-bond interaction, $\sigma_{hb} = 0.0084$ e A$^{-2}$.

value of $\sigma < -\sigma_{hb}$ shows affinity toward HBD, whereas the value of $\sigma > +\sigma_{hb}$ shows affinity toward HBA.

Figure 7 depicts peaks for TBPBr/EG and TBABr/EG on both sides ($\sigma > +\sigma_{hb}$ and $\sigma < -\sigma_{hb}$), which indicates that they are able to act either as HBD or as HBA. However, peaks on $\sigma > +\sigma_{hb}$ are significantly higher, making it a better HBA. This is in agreement with their respective $\sigma$ potential as in Figure 8, where the value of $\mu(\sigma)$ is more negative on the $\sigma < -\sigma_{hb}$ side compared to the $\sigma > +\sigma_{hb}$ side, indicating a higher affinity toward HBD.

Indoline is a weak HBD, whereas pyridine is a weak HBA. Indoline possesses a low peak at $\sigma < -\sigma_{hb}$, whereas pyridine possesses a small peak at $\sigma > +\sigma_{hb}$ (Figure 8). This can be subsequently proved by looking at the $\sigma$-potential of these two solutes. Pyridine shows a very high affinity toward HBD, whereas indoline has an affinity toward HBA (Figure 8). DBT, on the other hand, possesses peaks in the nonpolar region only (Figure 7). This means that DBT has no ability to form a hydrogen bonding with any of the solvents, thus only

interacting with the solvent via a nonpolar interaction, i.e., van der Waals interaction. The value of $\mu(\sigma)$ for DBT in Figure 8 is also parabolic in nature, where it shows a repulsive behavior toward other components. To combat this issue, solvent with peaks $\sigma < 0$ is favored to allow interaction between the solvent and the DBT peak.

**2.3. Experimental Liquid−Liquid Equilibrium (LLE) Data of Quinary Systems.** The results of the experimental tie lines for all quinary systems obtained at atmospheric pressure and room temperature are listed in Table 3. These experiments were triplicated, and the standard deviation was calculated. The triplicate results and calculated standard deviation can be found in Tables S4−S7 in the Supporting Information. Pseudo-ternary diagrams for both quinary systems were also plotted and are represented in Figures 9 and 10. This follows the work of Santiago and Aznar, where three quinary systems were presented by pseudo-ternary graphs.[37] The quinary systems investigated were TBPBr/EG (1) + pyridine (2) + indoline (3) + DBT (4) + n-hexadecane

**Table 3. LLE Tie Line for Quinary Systems at $T$ = 298.15 K and $P$ = 1 atm[a]**

| DES-rich phase | | | | | | hexadecane-rich phase | | | | | |
| --- | --- | --- | --- | --- | --- | --- | --- | --- | --- | --- | --- |
| $x'_1$ | $x'_2$ | $x'_3$ | $x'_4$ | $x'_0$ | $x'_5$ | $x''_1$ | $x''_2$ | $x''_3$ | $x''_4$ | $x''_0$ | $x''_5$ |
| TBPBr/EG (1:2) (1) + Pyridine (2) + Indoline (3) + DBT (4) + Hexadecane (5) | | | | | | | | | | | |
| 0.886 | 0.040 | 0.044 | 0.018 | 0.101 | 0.012 | 0.000 | 0.005 | 0.001 | 0.007 | 0.012 | 0.988 |
| 0.846 | 0.063 | 0.060 | 0.026 | 0.149 | 0.006 | 0.000 | 0.009 | 0.001 | 0.015 | 0.024 | 0.976 |
| 0.792 | 0.088 | 0.080 | 0.035 | 0.203 | 0.005 | 0.000 | 0.015 | 0.001 | 0.025 | 0.040 | 0.960 |
| 0.735 | 0.118 | 0.096 | 0.046 | 0.259 | 0.006 | 0.000 | 0.019 | 0.001 | 0.031 | 0.050 | 0.950 |
| 0.686 | 0.138 | 0.115 | 0.053 | 0.307 | 0.007 | 0.000 | 0.028 | 0.001 | 0.058 | 0.088 | 0.912 |
| 0.596 | 0.180 | 0.146 | 0.070 | 0.396 | 0.009 | 0.000 | 0.043 | 0.002 | 0.065 | 0.109 | 0.891 |
| TBABr/EG (1:2) (1) + Pyridine (2) + Indoline (3) + DBT (4) + Hexadecane (5) | | | | | | | | | | | |
| 0.881 | 0.028 | 0.030 | 0.015 | 0.073 | 0.046 | 0.000 | 0.004 | 0.001 | 0.008 | 0.013 | 0.987 |
| 0.847 | 0.045 | 0.048 | 0.021 | 0.115 | 0.037 | 0.000 | 0.007 | 0.001 | 0.013 | 0.021 | 0.979 |
| 0.822 | 0.057 | 0.059 | 0.028 | 0.143 | 0.035 | 0.000 | 0.010 | 0.001 | 0.020 | 0.031 | 0.969 |
| 0.770 | 0.083 | 0.083 | 0.039 | 0.205 | 0.025 | 0.000 | 0.017 | 0.001 | 0.035 | 0.053 | 0.947 |
| 0.740 | 0.098 | 0.095 | 0.045 | 0.237 | 0.022 | 0.000 | 0.017 | 0.001 | 0.041 | 0.059 | 0.941 |
| 0.691 | 0.118 | 0.113 | 0.054 | 0.285 | 0.025 | 0.000 | 0.039 | 0.001 | 0.049 | 0.089 | 0.911 |

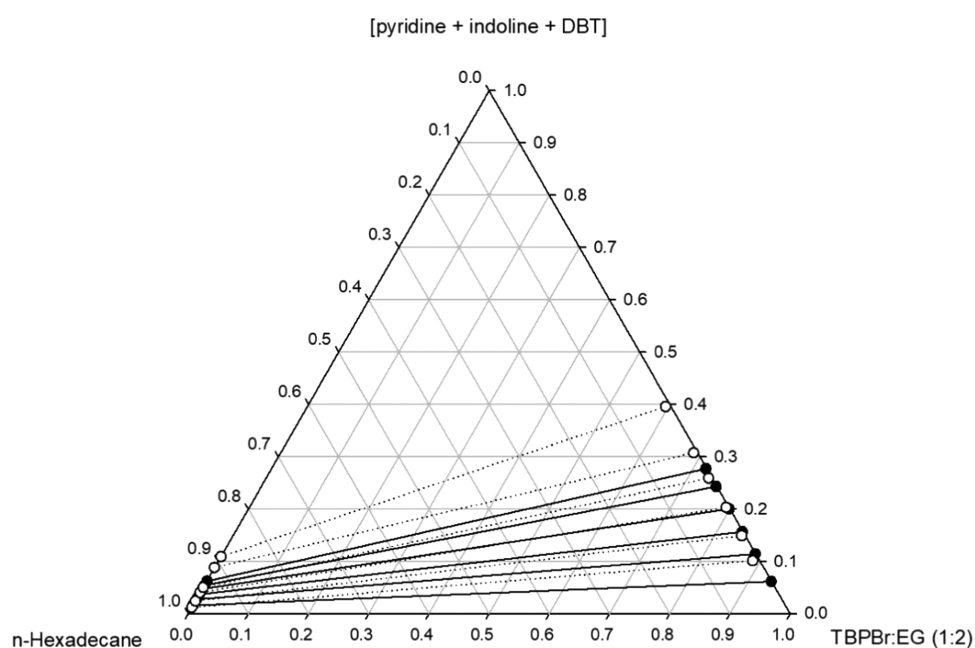[a]$x'_0 = x'_2 + x'_3 + x'_4$; $x''_0 = x''_2 + x''_3 + x''_4$.



**Figure 9.** Pseudo-ternary diagram for the quinary system TBPBr/EG (1) + pyridine (2) + indoline (3) + DBT (4) + $n$-hexadecane (5) at $T$ = 298.15 K and $P$ = 1 atm. Full circles solid lines, COSMO-RS tie lines; empty circles dashed-lines, experimental tie lines.

(5) and TBABr/EG (1) + pyridine (2) + indoline (3) + DBT (4) + $n$-hexadecane (5). Othmer−Tobias and Hand empirical correlations were used to assess the consistency of the experimental results. Linearity, $R^2$, close to 1 indicates the consistency of the experimental data, as shown in Table 4.

Results in Table 3 and Figures 9 and 10 show zero cross-contamination. This can prevent loss of the solvent during the extraction process. Apart from that, the amount of hexadecane found in the extract phase can be considered insignificant since the highest mole fraction found was 0.5, which is in TBABr/EG. This low affinity of hexadecane toward the solvents will increase the number of uses before any need for purification arises.

Figures 9 and 10 show that all systems possessed positive slopes for all of the tie lines. This demonstrates the high affinity of solutes toward the solvent than $n$-hexadecane. Other than that, based on Table 3, it is observed that among all three

solutes (pyridine, indoline, and DBT), the concentration of DBT is the highest in the raffinate phase followed by pyridine and indoline. This high concentration of DBT in the raffinate phase implies a higher amount of solvent required to extract DBT from hexadecane as the mixture increases from 5 to 30 wt %.[16]

From COSMO-RS screening, the orders of $S^\infty$ and $C^\infty$ are the highest for pyridine, followed by indoline and finally dibenzothiophene. However, from the experimental results, it was observed that the distribution ratio (reflective of capacity) and the selectivity of individual solute (refer to Tables S8 and S9 in the Supporting Information), the values are the highest for indoline, followed by pyridine and dibenzothiophene. This is also consistent with our previous work using the same DESs with individual nitrogen compounds, where both DESs show higher values of $S^\infty$ and $C^\infty$ for pyridine than for indoline from COSMO-RS screening, but in the experimental LLE, the
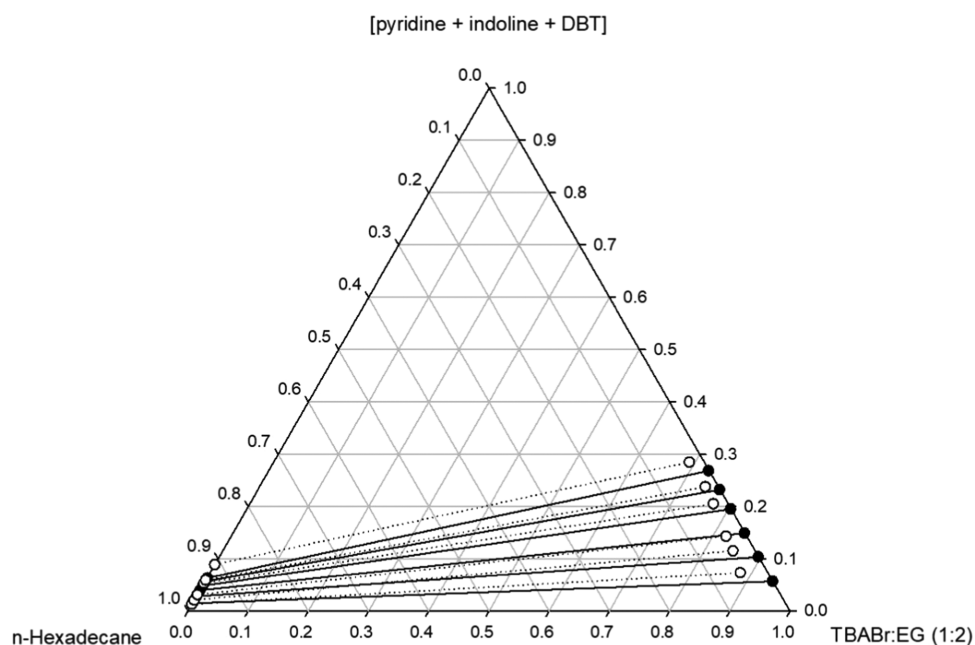
**Figure 10.** Pseudo-ternary diagram for the quinary system TBABr/EG (1) + pyridine (2) + indoline (3) + DBT (4) + *n*-Hexadecane (5) at *T* = 298.15 K and *P* = 1 atm. Full circles solid lines: COSMO-RS tie lines; empty circles dashed-lines: experimental tie lines.

**Table 4. Othmer−Tobias and Hand Parameters**

| | Othmer−Tobias | | | Hand | | |
|---|---|---|---|---|---|---|
| system | *a* | *b* | $R^2$ | *c* | *d* | $R^2$ |
| TBPBr/EG (1:2) + (pyridine + indoline + DBT) + hexadecane | 1.391 | −1.426 | 0.974 | 1.330 | −1.445 | 0.981 |
| TBABr/EG (1:2) + (pyridine + indoline + DBT) + hexadecane | 1.666 | −0.960 | 0.993 | 1.246 | −1.275 | 0.993 |

distribution ratio and selectivity are higher for indoline than for pyridine.[16,31] Although the COSMO-RS screening results and the experimental LLE results differ in the trend of which the nitrogen compound has a better selectivity and capacity (or distribution ratio) with DESs, it does not discount the ability of COSMO-RS to be used as a preliminary screening tool to select the most appropriate combinations of salt and HBD to be used as the extracting solvent for denitrogenation and desulfurization. The DESs also demonstrate that DBT as a sulfur compound has the lowest values of selectivity and capacity (or distribution ratio) compared to the nitrogen compounds both through COSMO-RS prediction and through experimental LLE.

An explanation as to why DBT has the lowest affinity and thus the lowest selectivity and capacity toward the DESs can be obtained from looking at its chemical structure and comparing it to that of pyridine and indoline. According to Table 8, it is apparent that DBT has a more complex structure than that of pyridine and indoline. This elaborated structure limits the interaction between DBT and the solvent due to the steric hindrance possessed by this compound, thus making it the most difficult solute to extract. Pyridine is a weaker hydrogen-bond acceptor compared to indoline, resulting in a weaker hydrogen bonding between pyridine and the DESs compared to indoline.

The predicted COSMO-RS tie line was plotted together with the experimental tie line and the root-mean-square deviation was used to evaluate the difference in fitting between these two tie lines using the following equation

$$\text{RMSD } (\%) = 100 \sqrt{\sum_{k=1}^{m} \sum_{i=1}^{c} \sum_{j=1}^{2} \frac{(x_{ik}^{j} - xc_{ik}^{j})^2}{2mc}} \tag{4}$$

where *x* is the mole fraction and subscripts *i*, *j*, *k*, and *m* are the component, phase, tie line, and number of tie lines, respectively. TBABr/EG has a lower deviation (2.29%) compared to TBPBr/EG (4.25%) between the COSMO-RS prediction and the experimental one showing good agreement between these two data. This can be clearly seen in Figure 10 where the tie lines of both predicted and experimental ones show a similar trend. The underestimation of COSMO-RS prediction for TBPBr/EG can be seen in Figure 9. However, an RMSD value below 5% is acceptable given the working principle of COSMO-RS, where the calculation of the energy interaction is solely based on its geometry structure.

**2.4. Distribution Coefficient, Selectivity, Extraction Capacity, and Extraction Affinity.** The distribution coefficient, *D*, and selectivity, *S*, are excellent parameters for determining the suitability of a solvent as an extractant. *D* demonstrates the distribution of a solute between the extract and raffinate phases, while *S* demonstrates the affinity of a solvent toward a solute. A magnitude of *D* and *S* higher than unity is desired as it indicates a good performance of the solvent. This helps the industry in cost reduction due to lowering of the solvent-to-feed ratio as well as the amount of solvent resulting in a smaller extraction column diameter and a reduced number of extraction stages.[38]

To make values of *D* and *S* more significant, parameters such as the extraction capacity, *α*, and the extraction affinity, *β*, were introduced. These two parameters are essentially *D* and *S* in

**Table 5. Overall Distribution Coefficient (D), Selectivity (S), Extraction Efficiency (α), and Extraction Affinity (β) of Solutes**

| TBPBr/EG (1:2) | | | | TBABr/EG (1:2) | | | |
|---|---|---|---|---|---|---|---|
| D | S | α (%) | β (%) | D | S | α (%) | β (%) |
| 8.19 | 661.3 | 89.12 | 99.85 | 5.75 | 123.74 | 85.18 | 99.20 |
| 6.18 | 1093.8 | 86.08 | 99.91 | 5.39 | 141.19 | 84.36 | 99.30 |
| 5.04 | 881.4 | 83.44 | 99.89 | 4.55 | 125.36 | 81.98 | 99.21 |
| 5.15 | 794.5 | 83.75 | 99.87 | 3.86 | 143.71 | 79.42 | 99.31 |
| 3.50 | 432.22 | 77.77 | 99.77 | 4.03 | 169.51 | 80.13 | 99.41 |
| 3.63 | 376.16 | 78.41 | 99.73 | 3.19 | 116.36 | 76.12 | 99.15 |

terms of percentage, and they help in comparing the performance of the three solvents.

$$D = \left(\frac{x_n'}{x_n''}\right) \tag{5}$$

$$S = \left(\frac{(x_n'/x_n'')}{(x_H'/x_H'')}\right) \tag{6}$$

$$\alpha = \left(\frac{x_n'}{x_n' + x_n''}\right) \times 100 \tag{7}$$

$$\beta = \left(\frac{\left(\frac{x_n'}{x_n'}\right)}{\left(\frac{x_H'}{x_H''}\right) + \left(\frac{x_n'}{x_n''}\right)}\right) \times 100 \tag{8}$$

where $n$ is 2 (pyridine), 3 (indoline), and 4 (DBT).

As shown in eq 5, $D$ is the ratio of the mole fraction of solutes in the extract to the mole fraction of solutes in raffinate, whereas $S$, as shown in eq 6, is the ratio of $D$ of solutes to $D$ of the carrier solvent, which in this case is $n$-hexadecane. $D$ and $S$ for each system were determined by calculating the average individual $D$ and $S$ contributed by each solute. Equation 7 calculates the extraction capacity, whereas eq 8 is the extraction affinity. Both eqs 7 and 8 were expressed in terms of percentage. Here, $x$ represents the mole fraction, whereas subscript $n$ represents the individual solutes present in $n$-hexadecane (pyridine, indoline, and DBT). ′ and ″ represent the extract and raffinate phases, respectively. Values for $D$, $S$, $α$, and $β$ are presented in Table 5, whereas the individual values can be found in Table S8 and S9 in the Supporting Information.

As can be seen in Table 5, $S$ and $D$ for all systems possess magnitude greater than 1. This shows a high affinity of solutes toward these solvents and a small amount of solvent required during the extraction process. The $α$ values for all solvents recorded at least 77% solute extraction, and this is consistent with the work done by Hizaddin et al.[31,38] This means that the presence of multiple solutes has a low effect on the extraction capability of these solvents. This is an improvement from a typical HDS process, where the presence of nitrogen usually affects the sulfur removal via deactivation of the catalyst.[39] Graphs of the distribution ratio and selectivity of multisolute in the raffinate phase were plotted (Figures 11 and 12). In this work, we have investigated the extraction performance of both ammonium- and phosphonium-based DESs. Various studies concerning the applications of different ammonium- and phosphonium-based DESs are summarized by our group.[40] The distribution ratio of TBPBr/EG and TBABr/EG shows a similar trend with a decreasing distribution ratio with the
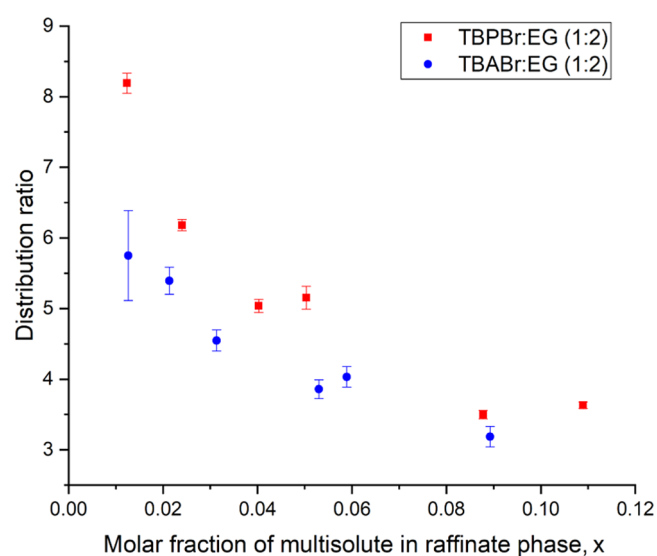


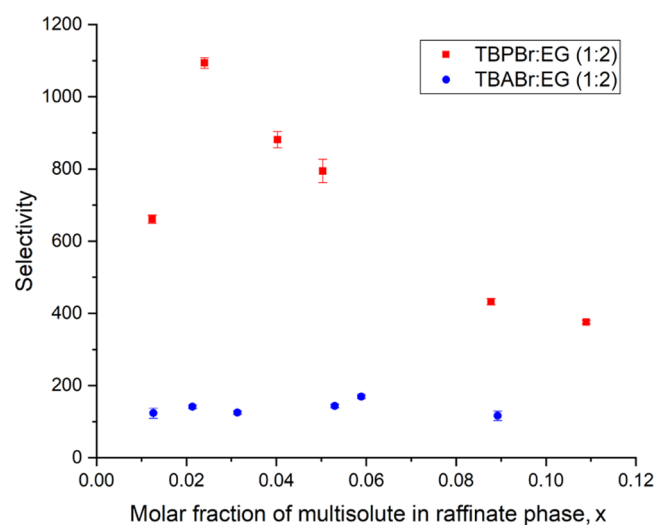**Figure 11.** Distribution ratio of multisolute in the raffinate phase.



**Figure 12.** Selectivity of multisolute in the raffinate phase.

increase of solute concentration with TBPBr/EG possessing a higher value. However, the difference of the value was insignificant except at 5 wt %.

Figure 12 shows the selectivity of the multisolute component in the raffinate phase. The trend for selectivity of TBPBr/EG is similar to the trend of the distribution ratio, where the selectivity decreases with an increase of the solute concentration. This is in line with the behavior of the distribution ratio, and it can be said that TBPBr/EG is a good extracting solvent at a low concentration of the solute. On the

**Table 6. Extraction Efficiency ($\alpha$) for Various Choline-Based DESs at Molar Ratio 1:2[a]**

| ILs/DESs | hydrocarbon | extraction type | solute | $\alpha$ (%) | references |
|---|---|---|---|---|---|
| TBPBr/EG | *n*-hexadecane | simultaneous-solute extraction | pyridine | 88.9[a] | this work |
| | | | indoline | 97.8[a] | this work |
| | | | DBT | 72.0[a] | this work |
| TBABr/EG | *n*-hexadecane | simultaneous-solute extraction | pyridine | 87.5[a] | this work |
| | | | pndoline | 96.8[a] | this work |
| | | | DBT | 52.4[a] | this work |
| ChCl/EG | simulated gasoline | simultaneous-solute extraction | pyridine | 60.0 | 24 |
| | | | thiophene | 35.0 | 24 |
| ChCl/U | *n*-heptane | extractive denitrogenation | pyridine | 6.50 | 41 |
| | | | carbazole | 40.1 | 41 |
| ChCl/G | *n*-heptane | extractive denitrogenation | pyridine | 51.4 | 41 |
| | | | carbazole | 78.9 | 41 |
| ChCl/PAA | *n*-heptane | extractive denitrogenation | pyridine | 99.2 | 41 |
| | | | carbazole | 98.2 | 41 |
| ChCl/PPA | *n*-heptane | extractive denitrogenation | pyridine | 96.3 | 41 |
| | | | carbazole | 97.9 | 41 |

[a]Pyridine and indoline at 5 wt % and DBT at 30 wt %.

**Table 7. Comparison of Selectivity ($S$), Distribution Coefficient (D), Extraction Capacity ($\alpha$), and Extraction Affinity ($\beta$) of Solutes[a]**

| DESs | hydrocarbon | extraction type | solute | $D$ | $S$ | $D$ (COSMO-RS) | $S$ (COSMO-RS) | $\alpha$ (%) | $\beta$ (%) | references |
|---|---|---|---|---|---|---|---|---|---|---|
| TBABr/EG | *n*-hexadecane | single-solute extraction | pyridine | 4.22 | 829 | | | 80.8 | 99.88 | 31 |
| | | | indoline | 7.57 | 2,506 | | | 88.3 | 99.90 | 31 |
| | | simultaneous-solute extraction | pyridine | 7.00 | 150.2 | 3.01 | 622.3 | 87.5 | 99.34 | this work |
| | | | indoline | 30.00 | 643.7 | 1.83 | 378.3 | 96.8 | 99.84 | this work |
| | | | DBT | 1.10 | 40.2 | 0.29 | 59.6 | 52.4 | 97.57 | this work |
| TBPBr/EG | *n*-hexadecane | single-solute extraction | pyridine | 3.74 | 244 | | | 78.9 | 99.59 | 31 |
| | | | indoline | 7.00 | 772 | | | 87.5 | 99.87 | 31 |
| | | simultaneous-solute extraction | pyridine | 8.00 | 658.7 | 3.15 | 508.0 | 88.9 | 99.85 | this work |
| | | | indoline | 44.00 | 3622.7 | 1.97 | 318.0 | 97.8 | 99.97 | this work |
| | | | DBT | 1.08 | 106.6 | 0.32 | 51.9 | 51.9 | 99.07 | this work |

[a]Pyridine and indoline at 5 wt % and DBT at 30 wt %.

other hand, the selectivity of TBABr/EG is similar at all solute concentrations. This steady behavior shows the low effect the multisolute has on TBABr/EG. It is also observed that the curve length of TBPBr/EG in both Figures 11 and 12 is slightly longer than that of TBABr/EG. This length reflects the efficiency of the extraction process, where a shorter curve indicates a higher efficiency.[7] This behavior of TBPBr/EG was contributed by the higher amount of solutes in the raffinate phase for TBPBr/EG despite having larger $\alpha$ values compared to TBABr/EG.

Table 6 shows the comparison of the extraction efficiency, $\alpha$, between various choline-based DESs from previous studies with the DESs used in this work. Among all of the DESs listed, only ChCl/EG was used in simultaneously extracting nitrogen and sulfur compounds. As observed in Table 6, $\alpha$ for this ChCl/EG recorded 60 and 35% extraction of pyridine and thiophene. On the other hand, the DESs used in this work recorded $\alpha$ values for pyridine and DBT of more than 87.5 and 52.4%. This implies that tetrabutyl-based salt works better in simultaneously extracting nitrogen and sulfur compounds.
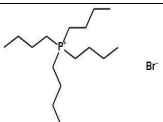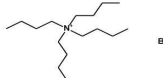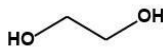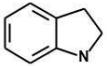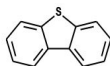
For the extraction of pyridine, ChCl/U and ChCl/G exhibited lower $\alpha$ values with 6.50 and 51.4%, respectively, in comparison to TBPBr/EG (88.9%) and TBABr/EG (87.5%). Meanwhile, ChCl/PAA (99.2%) and ChCl/PPA (96.3%) showed higher $\alpha$ values than TBPBr/EG and TBABr/

EG. Although ChCl/PAA and ChCl/PPA have higher $\alpha$ values, the absence of the sulfur compound might contribute to these results. As shown in Figure 3, choline-based DESs generally have a lower capacity compared to DESs based on other compounds. This implies that the presence of the sulfur compound might reduce the performance of these DESs in simultaneously extracting both sulfur and nitrogen compounds.

**2.5. Effect of Multiple-Solute Extraction on the Performance of the Solvents.** The effect of the sulfur compound and multiple solutes on the extraction performance of the solvent was investigated by comparing the results obtained from this work with the previous work done by our group on the single extraction of the nitrogen compound.[31] From Table 7, it can be seen that both single-solute extraction and simultaneous-solute extraction yield the same extraction pattern where DBT has the lowest extraction capacity, followed by pyridine and then indoline. This is in line with an earlier explanation where DBT has the highest steric hindrance resulting in a poor interaction with the solvent, whereas pyridine is a weaker hydrogen-bond acceptor compared to indoline.

Apart from that, Table 7 also shows the difference in the extraction capacity, $\alpha$, and extraction affinity, $\beta$, of these solutes during a single-solute extraction and multiple-solute extraction. The comparison for the nitrogen compound was made at 5 wt

**Table 8. List of Chemicals Used in This Study**

| Name | Chemical Formula | Structure | Purity | Supplier |
|---|---|---|---|---|
| TBPBr | $C_{16}H_{36}BrP$ | | ≥ 98.0 | Sigma-Aldrich (Germany) |
| TBABr | $C_{16}H_{36}BrN$ | | ≥ 98.0 | Sigma-Aldrich (Germany) |
| EG | $C_2H_6O_2$ | | 99.8 | Sigma-Aldrich (Germany) |
| Hexadecane | $CH_3(CH_2)_{14}CH_3$ | | ≥ 99.0 | Sigma-Aldrich (Germany) |
| Pyridine | $C_5H_5N$ | | 99.8 | Sigma-Aldrich (Germany) |
| Indoline | $C_8H_9N$ | | 99.0 | Sigma-Aldrich (China) |
| DBT | $C_{12}H_8S$ | | ≥ 98.0 | Sigma-Aldrich (Germany) |
| Chloroform-D1 | $CDCl_3$ | | ≥ 99.8 | Sigma-Aldrich (Germany) |
| Dodecane | $C_{12}H_{16}$ | | ≥ 99.0 | Sigma-Aldrich (Germany) |

% and sulfur was taken at 30 wt %. The choice of the weight percent is to reflect the amount of nitrogen and sulfur compounds found in real fuel oil as reported in the literature.[3,42] The extraction capacity of indoline and pyridine is higher during a multisolute extraction when compared to during a single-solute extraction. This shows that not only the presence of sulfur did not affect the extraction of nitrogen compounds but also the extraction of the multisolute compound is more efficient than a single-solute compound.

The distribution coefficient, $D$, for experimental data exhibited higher values compared to the values by COSMO-RS, especially for the case of indoline, where the predicted $D$ value showed significantly lower values (TBABr/EG: 1.83 and TBPBr/EG: 1.97) compared to the experimental results (TBABr/EG: 30.0; TBPBr/EG: 44.0). This can also be seen in Figures 9 and 10 where the experimental tie lines exhibit a higher slope than the tie lines of the predicted COSMO-RS. This shows the underestimation of capacity for both TBPBr/EG and TBABr/EG by COSMO-RS.

Selectivity values, $S$, of TBPBr/EG follow the trend of $D$ values where experimental results are higher than those of the COSMO-RS predictions. This is shown in Figure 9, where it can be clearly seen that zero amount of n-hexadecane is found in TBPBr/EG. On the other hand, a trace amount of n-hexadecane can be found in TBABr/EG as opposed to the COSMO-RS prediction tie line, which explains the lower experimental $S$ values for the TBABr/EG system (Figure 10). However, the deviations between the predicted COSMO-RS (TBABr/EG: 2.29%; TBPBr/EG: 4.25%) and experimental tie

lines were lower than 5%, which indicates the ability of COSMO-RS in predicting equilibrium data.

## 3. CONCLUSIONS

The ability of two DESs, namely, TBPBr/EG and TBABr/EG, to extract multiple solutes (pyridine, indoline, and DBT) simultaneously from n-hexadecane was evaluated and presented in phase diagrams. There was zero cross-contamination between the solvent and n-hexadecane, making these solvents a good extractant solvent. All phase diagrams possessed a positive slope, indicating the small amount of solvent required to extract solutes from n-hexadecane. Performances of these solvents were calculated from their selectivity ($S$), distribution coefficient ($D$), extraction capacity ($\alpha$), and extraction affinity ($\beta$). Extraction capacity and extraction affinity are just essentially percentage values of selectivity and the distribution coefficient and were introduced for ease of comparison among all three solvents. Based on the results obtained, TBPBr/EG shows the highest $\alpha$ range of 89.1−78.4% followed by TBABr/EG with 85.2−76.1%. It was also observed that TBPBr/EG has a higher $\alpha$ value compared to TBABr/EG at all concentrations except at 25 wt %. The $\alpha$ value decreases with the increase of the solute weight percent except at 25 wt % solute. This is in line with the COSMO-RS screening results, where TBPBr/EG demonstrates higher values of capacity at infinite dilution than TBABr/EG. This work shows promising results for sulfur and nitrogen separation. Even though it cannot replace the hydrotreating process entirely, this simple extraction process can be introduced as a pretreatment process. This may help in

prolonging the catalyst used in the hydro process due to the reduced number of nitrogen and sulfur compounds. RMSD for COSMO-RS calculated is less than 5%. It is safe to say that COSMO-RS is a good tool for the preliminary test in solvent prediction. The low deviation percentage between COSMO-RS and experimental data shows the ability of COSMO-RS to correctly predict the extraction capability of a certain solvent.

## 4. MATERIALS AND METHODS

**4.1. Materials.** The chemicals used in this work are listed in Table 8 along with their purity, origin, and chemical structure. Dodecane was used in gas chromatography (GC) to determine the composition of the extract and raffinate phases. Deuterated chloroform ($CDCl_3$) was used in $^1H$ NMR spectroscopy analysis. DESs used in this work were synthesized, whereas other chemicals, i.e., pyridine, indoline, dibenzothiophene, and hexadecane, were used as received without further purification.

**4.2. Screening of Deep Eutectic Solvents via COSMO-RS.** The conductor-like screening model for real solvents (COSMO-RS) has been used as a solvent screening tool in the past decade. It is a quantum chemical calculation approach paired with statistical thermodynamics[16] used to predict the behavior of the liquid without requiring experimental data. This is exceptionally useful for solvents like ILs and DESs, which have limited data available for experimental physical and chemical properties.

Behavioral prediction of liquid mixtures can be achieved in COSMO-RS by converging the geometry and electron density to its optimal energy state, which will be the reference for other thermodynamic calculations. It is done in a perfect conductor state instead of an exact dielectric boundary condition, which enables COSMO-RS to achieve the results predictively at any temperature. This calculation will result in the distribution of screening charge density, which is then converted into a function of surface composition. This screening charged density will generate an output known as the. *cosmo* file where the statistical thermodynamic principle will be applied to calculate other important parameters, which are the molecular energy. This calculated molecular energy is based on the van der Waals force, electrostatic misfit, and hydrogen bond of the molecules.[30,43]

The screening charge densities, also known as the $\sigma$-profiles, describe the relative amount of surface with polarity $\sigma$ for a molecule X. This information is sufficient for the COSMO-RS statistical thermodynamics calculations, where $\sigma$-profiles for solvents—pure or mixed—can be easily derived from the molecular $\sigma$-profiles obtained. It is derived as the mole fraction weighted sum of the $\sigma$-profiles of its compounds combined with a surface normalization as written in the following equation

$$p_s(\sigma) = \frac{\sum_i x_i p^{x_i}(\sigma)}{\sum_i x_i A^{x_i}} \tag{9}$$

The most relevant energy contribution for molecular interaction is from electrostatics $E_{misfit}$ and hydrogen bonding $E_{HB}$, whereas van der Waals ($E_{vdW}$) is taken into account in an approximate way. Electrostatics $E_{misfit}$ and hydrogen bonding $E_{HB}$ are described as functions of screening charges, which are $\sigma_{acceptor}$ and $\sigma_{donor}$.

$$E_{misfit}(\sigma, \sigma') = a_{eff}\frac{\alpha'}{2}(\sigma + \sigma')^2 \tag{10}$$

$$E_{HB} = a_{eff}c_{HB} \min(0; (0; \sigma_{donor} + \sigma_{HB})$$
$$(0; \sigma_{acceptor} - \sigma_{HB})) \tag{11}$$

$$E_{vdW} = a_{eff}(\tau_{vdW} + \tau'_{vdW}) \tag{12}$$

The chemical potential of the surface can be calculated using the following equation

$$\mu_S(\sigma) = -RT \ln\left[\int ps\left(\left(\sigma'\right)\exp\left(\frac{1}{RT}(a_{eff}\mu_S(\sigma')\right.\right.\right.$$
$$\left.\left.\left. - E_{misfit}(\sigma, \sigma') - E_{HB}(\sigma, \sigma')\right)\right)d\sigma'\right] \tag{13}$$

where $\mu_S(\sigma)$ is the $\sigma$-potential, which describes the affinity of a solvent toward the surface polarity, $\sigma$. By integrating the $\mu_S(\sigma)$ over the surface of the compound, the pseudo-chemical potential of solute X in solvent S can be obtained using the following calculation[40]

$$\mu_S^X = \mu_{C,S}^X + \int p^{X_i}(\sigma)\mu_S(\sigma)\,d\sigma \tag{14}$$

COSMO-RS was used in this work as a screening tool by estimating the activity coefficient of each DES in extracting nitrogen and sulfur compounds. Forty-four DESs were screened, and their respective selectivity, capacity, and performance index were calculated and evaluated to choose the best DESs to simultaneously extract nitrogen and sulfur compounds from diesel fuel oil. The list of DESs screened can be found in Table S2 in the Supporting Information. First, the chemical structures of all DESs, solvents, and solutes were optimized using TurbomoleX performed at the 6-31G* basis set at the Hartree−Fock level. After that, a single-point calculation was performed using DFT and Becke−Perdew methods together with the triple $\zeta$ valence potential (TZVP) basis set to generate the. *cosmo* files. Lastly, the generated. *cosmo* files will be exported to the COSMOthermX program to be used in the computation of molecular energy by applying statistical thermodynamic principles.

**4.3. Molecule Representation in COSMO-RS.** Since ionic DES is made up of more than one molecule, an accurate representation is very important. There are three approaches that can be used in representing DESs in COSMO-RS, which are (i) the metafile approach, (ii) the ion-pair approach, and (iii) the electroneutral approach. Among these three approaches, the third approach has the closest representation of DES as in nature where both anions and cations are treated as two individual compounds in an equimolar mixture. On the other hand, the first approach treats ions differently in COSMO calculations but later combines the calculation into a file known as metafile in the COSMO-RS calculation and the second approach uses an optimized ion-pair structure.

**4.4. Synthesis of Deep Eutectic Solvents.** DESs used in this work were synthesized using the same method reported in our previous work that follows the method described by Abbott et al., where salt and HBD with specific molar ratios were mixed.[17,31,32] The two DESs used in this work are TBPBr/EG and TBABr/EG at a salt/HBD molar ratio of 1:2, respectively. A mixture of 15 g of salt (TBPBr or TBABr) with its corresponding HBD (EG) was weighed using a Mettler

Toledo balance with an accuracy of 0.001 g. These DES mixtures were mixed in 100 mL blue cap bottles and stirred on a hot-plate magnetic stirrer at a temperature of 80 °C and 200 rpm until homogenous liquids were formed. The blue cap bottles were sealed with Parafilm tape to avoid moisture contamination and loss to the surrounding. The stabilities of these DESs were observed by leaving them at room temperature for 24 h.

**4.5. Preparation of Diesel Fuel Sample and Liquid−Liquid Extraction.** For this work, hexadecane was chosen as the representative of diesel fuel oil, indoline and pyridine represented nitrogen compounds, and dibenzothiophene was the representative for sulfur compounds. The diesel fuel sample was fixed at 3 g, whereas the concentrations of the solute were varied from 5 to 30 wt % with an equivalent mass of indoline, pyridine, and dibenzothiophene. Other than that, an equal ratio of indoline, pyridine, and dibenzothiophene was used for ease of experimental measurement. The solvents were added to the feed mixture at a feed-to-solvent ratio of 1:1 in 20 mL glass scintillation vials. The samples were shaken at room temperature and atmospheric pressure for 5 h and left to settle for at least 12 h to ensure complete phase separation prior to further analysis.

**4.6. Compositional Analysis by GC.** A Trace GC-2010 (Shimadzu) system consisting of a flame ionization detector (FID) and an HP-5 column (5% diphenyl/95% dimethylpo-lysiloxane, 30 m, 0.32 mm, 0.25 $\mu$m) was used for the characterization. Helium with a split mode was used as a carrier gas. To measure the composition, dodecane was used as an external standard and calibration curves of sulfur and nitrogen compounds/dodecane were plotted (Figure S1). Furthermore, the optimum conditions of GC analysis for sulfur and nitrogen compounds/hexadecane system are provided in Table 9. We triplicated each experimental measurement, and

**Table 9. Gas Chromatography Operating Conditions**

| parameter | |
|---|---|
| temperature of injector (K) | 538.15 |
| temperature of detector (K) | 573.15 |
| carrier gas pressure (kPa) | 100 |
| oven program | 313.15 K for 4 min |
| | 313.15− 373.15 K |
| | rate: 15 K/min, hold time: 2 min |
| | 373.15−573.15 K |
| | rate: 45 K/min, hold time: 2 min |

the reported average uncertainty in molar compositions was estimated to be ±0.005. To confirm the absence of the DESs in the top layer, samples from this layer were analyzed by $^1$H NMR spectroscopy (Figures S2 and S3).

A total of 60 $\mu$L was taken from the extract and raffinate layer to be dissolved in 0.7 mL of CDCl$_3$ into an NMR tube using a pipette. A sample of the extract layer was purged to avoid any contamination by the raffinate layer. The mixture was shaken until it was fully dissolved in CDCl$_3$, and the cap was sealed with parafilm to avoid any loss and contamination. The samples were analyzed using $^1$H NMR Bruker Ultrashield Plus (400 MHz), where the hydrogen peaks of the mixtures were measured. The peak of pure components and the mixture of known concentrations were used to help select identification peaks for calculation purposes.

**4.7. Consistency Tests.** The Othmer−Tobias and Hand correlations were used to test the consistency of the quinary experimental data using eqs 15 and 16.[43]

$$\ln\left(\frac{1 - x''_{\mathrm{H}}}{x''_{\mathrm{H}}}\right) = a + b \ln\left(\frac{1 - x'_{\mathrm{SV}}}{x'_{\mathrm{SV}}}\right) \tag{15}$$

$$\ln\left(\frac{x''_{\mathrm{SU}}}{x''_{\mathrm{H}}}\right) = c + d \ln\left(\frac{x'_{\mathrm{SU}}}{x'_{\mathrm{SV}}}\right) \tag{16}$$

$x_{\mathrm{H}}$, $x_{\mathrm{SV}}$, and $x_{\mathrm{SU}}$ refer to the mole fraction of hexadecane, solvent, and solutes, respectively, whereas $'$ and $''$ refer to extract and raffinate phases, respectively. $a$, $b$, $c$, and $d$ are the Othmer−Tobias and Hand fitting parameters, where linearity ($R^2$) close to unity indicates high consistency of the experimental data.[38]

## ■ ASSOCIATED CONTENT

**ⓢ Supporting Information**

The Supporting Information is available free of charge at https://pubs.acs.org/doi/10.1021/acsomega.1c03034.

> List of screened DESs, chemical structure of DES cations, triplicate of LLE data, GC calibration curves, selectivity and distribution coefficient for individual solutes, $^1$H NMR spectra of pure DES, and a sample of the top layer of the extraction experiment (PDF)

## ■ AUTHOR INFORMATION

**Corresponding Authors**

**Hanee F. Hizaddin** − *Department of Chemical Engineering, Faculty of Engineering, Universiti Malaya, 50603 Kuala Lumpur, Malaysia; University of Malaya Centre for Ionic Liquids (UMCiL), Universiti Malaya, 50603 Kuala Lumpur, Malaysia;* ⓞ orcid.org/0000-0002-4119-8282; Email: hanee@um.edu.my

**Mohamed K. Hadj-Kali** − *Chemical Engineering Department, King Saud University, Riyadh 11421, Saudi Arabia;* ⓞ orcid.org/0000-0002-1374-9825; Email: mhadjkali@ksu.edu.sa

**Authors**

**Hurun E. Suhaimi** − *Department of Chemical Engineering, Faculty of Engineering, Universiti Malaya, 50603 Kuala Lumpur, Malaysia; University of Malaya Centre for Ionic Liquids (UMCiL), Universiti Malaya, 50603 Kuala Lumpur, Malaysia*

**Irfan Wazeer** − *Chemical Engineering Department, King Saud University, Riyadh 11421, Saudi Arabia*

**Lahssen El Blidi** − *Chemical Engineering Department, King Saud University, Riyadh 11421, Saudi Arabia*

**Mohd A. Hashim** − *Department of Chemical Engineering, Faculty of Engineering, Universiti Malaya, 50603 Kuala Lumpur, Malaysia; University of Malaya Centre for Ionic Liquids (UMCiL), Universiti Malaya, 50603 Kuala Lumpur, Malaysia*

Complete contact information is available at:
https://pubs.acs.org/10.1021/acsomega.1c03034

**Notes**

The authors declare no competing financial interest.

## ■ REFERENCES

(1) Ali, M. F.; Al-Malki, A.; Ahmed, S. Chemical desulfurization of petroleum fractions for ultra-low sulfur fuels. *Fuel Process. Technol.* **2009**, *90*, 536−544.

(2) El Sayed, H. A.; El Naggar, A. M. A.; Heakal, B. H.; Ahmed, N. E.; Said, S.; Abdel-Rahman, A. A. H. Deep catalytic desulphurization of heavy gas oil at mild operating conditions using self-functionalized nanoparticles as a novel catalyst. *Fuel* **2017**, *209*, 127−131.

(3) Prado, G. H. C.; Rao, Y.; de Klerk, A. Nitrogen Removal from Oil: A Review. *Energy Fuels* **2017**, *31*, 14−36.

(4) Nancarrow, P.; Mustafa, N.; Shahid, A.; Varughese, V.; Zaffar, U.; Ahmed, R.; Akther, N.; Ahmed, H.; AlZubaidy, I.; Hasan, S.; Elsayed, Y.; Sara, Z. Technical Evaluation of Ionic Liquid-Extractive Processing of Ultra Low Sulfur Diesel Fuel. *Ind. Eng. Chem. Res.* **2015**, *54*, 10843−10853.

(5) Lima, F.; Dave, M.; Silvestre, A. J. D.; Branco, L. C.; Marrucho, I. M. Concurrent Desulfurization and Denitrogenation of Fuels Using Deep Eutectic Solvents. *ACS Sustainable Chem. Eng.* **2019**, *7*, 11341−11349.

(6) Xu, H.; Zhang, D.; Wu, F.; Wei, X.; Zhang, J. Deep desulfurization of fuels with cobalt chloride-choline chloride/polyethylene glycol metal deep eutectic solvents. *Fuel* **2018**, *225*, 104−110.

(7) Salleh, M. Z. M.; Hadj-Kali, M. K.; Hizaddin, H. F.; Ali Hashim, M. Extraction of nitrogen compounds from model fuel using 1-ethyl-3-methylimidazolium methanesulfonate. *Sep. Purif. Technol.* **2018**, *196*, 61−70.

(8) Wu, Z.; Ondruschka, B. Ultrasound-assisted oxidative desulfurization of liquid fuels and its industrial application. *Ultrason. Sonochem.* **2010**, *17*, 1027−1032.

(9) Ja'fari, M.; Ebrahimi, S. L.; Khosravi-Nikou, M. R. Ultrasound-assisted oxidative desulfurization and denitrogenation of liquid hydrocarbon fuels: A critical review. *Ultrason. Sonochem.* **2018**, *40*, 955−968.

(10) Shah, S. S.; Ahmad, I.; Ahmad, W.; Ishaq, M.; Khan, H. Deep Desulphurization Study of Liquid Fuels Using Acid Treated Activated Charcoal as Adsorbent. *Energy Fuels* **2017**, *31*, 7867−7873.

(11) Balinge, K. R.; Khiratkar, A. G.; Krishnamurthy, M.; Patle, D. S.; Cheralathan, K. K.; Bhagat, P. R. Deep-desulfurization of the petroleum diesel using the heterogeneous carboxyl functionalized poly-ionic liquid. *Resour.-Effic. Technol.* **2016**, *2*, S105−S113.

(12) Liu, J.; Ma, B. Removal of Nitrogen Compounds from Shale Diesel Fraction Using Ionic Liquid [C4mim]HSO4. *China Pet. Process. Petrochem. Technol.* **2016**, 15−21.

(13) Mguni, L. L.; Yao, Y.; Liu, X.; Yuan, Z.; Hildebrandt, D. Ultra-deep desulphurization of both model and commercial diesel fuels by adsorption method. *J. Environ. Chem. Eng.* **2019**, *7*, No. 102957.

(14) Palomeque-Santiago, J. F.; López-Medina, R.; Oviedo-Roa, R.; Navarrete-Bolaños, J.; Mora-Vallejo, R.; Montoya-de la Fuente, J. A.; Martínez-Magadán, J. M. Deep oxidative desulfurization with simultaneous oxidative denitrogenation of diesel fuel and straight run gas oil. *Appl. Catal., B* **2018**, *236*, 326−337.

(15) Tang, X.-d.; Zhang, Y.-f.; Li, J.-j.; Zhu, Y.-q.; Qing, D.-y.; Deng, Y.-x. Deep Extractive Desulfurization with Arenium Ion Deep Eutectic Solvents. *Ind. Eng. Chem. Res.* **2015**, *54*, 4625−4632.

(16) Hizaddin, H. F.; Ramalingam, A.; Hashim, M. A.; Hadj-Kali, M. K. O. Evaluating the Performance of Deep Eutectic Solvents for Use in Extractive Denitrification of Liquid Fuels by the Conductor-like Screening Model for Real Solvents. *J. Chem. Eng. Data* **2014**, *59*, 3470−3487.

(17) Abbott, A. P.; Boothby, D.; Capper, G.; Davies, D. L.; Rasheed, R. K. Deep Eutectic Solvents Formed between Choline Chloride and Carboxylic Acids: Versatile Alternatives to Ionic Liquids. *J. Am. Chem. Soc.* **2004**, *126*, 9142−9147.

(18) Dai, Y.; van Spronsen, J.; Witkamp, G.-J.; Verpoorte, R.; Choi, Y. H. Ionic Liquids and Deep Eutectic Solvents in Natural Products Research: Mixtures of Solids as Extraction Solvents. *J. Nat. Prod.* **2013**, *76*, 2162−2173.

(19) Tang, B.; Row, K. H. Recent developments in deep eutectic solvents in chemical sciences. *Monatsh. Chem.* **2013**, *144*, 1427−1454.

(20) Kareem, M. A.; Mjalli, F. S.; Hashim, M. A.; Hadj-Kali, M. K.O.; Bagh, F. S. G.; Alnashef, I. M. Phase equilibria of toluene/heptane with tetrabutylphosphonium bromide based deep eutectic solvents for the potential use in the separation of aromatics from naphtha. *Fluid Phase Equilib.* **2012**, *333*, 47−54.

(21) Gao, S.; Li, J.; Chen, X.; Abdeltawab, A. A.; Yakout, S. M.; Yu, G. A combination desulfurization method for diesel fuel: Oxidation by ionic liquid with extraction by solvent. *Fuel* **2018**, *224*, 545−551.

(22) Laredo, G. C.; Likhanova, N. V.; Lijanova, I. V.; Rodriguez-Heredia, B.; Castillo, J. J.; Perez-Romo, P. Synthesis of ionic liquids and their use for extracting nitrogen compounds from gas oil feeds towards diesel fuel production. *Fuel Process. Technol.* **2015**, *130*, 38−45.

(23) Darwish, A. S.; Abu Hatab, F.; Lemaoui, T.; Ibrahim, O. A. Z.; Almustafa, G.; Zhuman, B.; Warrag, S. E. E.; Hadj-Kali, M. K.; Benguerba, Y.; Alnashef, I. M. Multicomponent extraction of aromatics and heteroaromatics from diesel using acidic eutectic solvents: Experimental and COSMO-RS predictions. *J. Mol. Liq.* **2021**, *336*, No. 116575.

(24) Rogošić, M.; Kučan, K. Z. Deep eutectic solvents based on choline chloride and ethylene glycol as media for extractive denitrification/desulfurization/dearomatization of motor fuels. *J. Ind. Eng. Chem.* **2019**, *72*, 87−99.

(25) de Riva, J.; Ferro, V. R.; Moreno, D.; Diaz, I.; Palomar, J. Aspen Plus supported conceptual design of the aromatic−aliphatic separation from low aromatic content naphtha using 4-methyl-N-butylpyridinium tetrafluoroborate ionic liquid. *Fuel Process. Technol.* **2016**, *146*, 29−38.

(26) Klamt, A.; Eckert, F. COSMO-RS: a novel and efficient method for the a priori prediction of thermophysical data of liquids. *Fluid Phase Equilib.* **2000**, *172*, 43−72.

(27) Salleh, Z.; Wazeer, I.; Mulyono, S.; El-blidi, L.; Hashim, M. A.; Hadj-Kali, M. K. Efficient removal of benzene from cyclohexane-benzene mixtures using deep eutectic solvents − COSMO-RS screening and experimental validation. *J. Chem. Thermodyn.* **2017**, *104*, 33−44.

(28) Naik, P. K.; Paul, S.; Banerjee, T. Liquid Liquid Equilibria measurements for the extraction of poly aromatic nitrogen hydro-carbons with a low cost Deep Eutectic Solvent: Experimental and theoretical insights. *J. Mol. Liq.* **2017**, *243*, 542−552.

(29) Warrag, S. E. E.; Adeyemi, I.; Rodriguez, N. R.; Nashef, I. M.; van Sint Annaland, M.; Kroon, M. C.; Peters, C. J. Effect of the Type of Ammonium Salt on the Extractive Desulfurization of Fuels Using Deep Eutectic Solvents. *J. Chem. Eng. Data* **2018**, *63* (4), 1088−1095.

(30) Gouveia, A. S. L.; Oliveira, F. S.; Kurnia, K. A.; Marrucho, I. M. Deep Eutectic Solvents as Azeotrope Breakers: Liquid−Liquid Extraction and COSMO-RS Prediction. *ACS Sustainable Chem. Eng.* **2016**, *4*, 5640−5650.

(31) Hizaddin, H. F.; Hadj-Kali, M. K.; Ramalingam, A.; Ali Hashim, M. Extractive denitrogenation of diesel fuel using ammonium- and phosphonium-based deep eutectic solvents. *J. Chem. Thermodyn.* **2016**, *95*, 164−173.

(32) Hernández-Bravo, R.; Miranda, A. D.; Martínez-Mora, O.; Domínguez, Z.; Martínez-Magadán, J. M.; García-Chávez, R.; Domínguez-Esquivel, J. M. Calculation of the Solubility Parameter by COSMO-RS Methods and Its Influence on Asphaltene−Ionic Liquid Interactions. *Ind. Eng. Chem. Res.* **2017**, *56* (17), 5107−5115.

(33) Larriba, M.; de Riva, J.; Navarro, P.; Moreno, D.; Delgado-Mellado, N.; García, J.; Ferro, V. R.; Rodríguez, F.; Palomar, J.

COSMO-based/Aspen Plus process simulation of the aromatic extraction from pyrolysis gasoline using the {[4empy][NTf2] + [emim][DCA]} ionic liquid mixture. *Sep. Purif. Technol.* **2018**, *190*, 211−227.

(34) González, E. J.; Palomar, J.; Navarro, P.; Larriba, M.; García, J.; Rodríguez, F. On the volatility of aromatic hydrocarbons in ionic liquids: Vapor-liquid equilibrium measurements and theoretical analysis. *J. Mol. Liq.* **2018**, *250*, 9−18.

(35) Ferro, V. R.; de Riva, J.; Sanchez, D.; Ruiz, E.; Palomar, J. Conceptual design of unit operations to separate aromatic hydro-carbons from naphtha using ionic liquids. COSMO-based process simulations with multi-component "real" mixture feed. *Chem. Eng. Res. Des.* **2015**, *94*, 632−647.

(36) Farghi, F.; Kaddami, M. Liquid−Liquid Equilibrium of the Quaternary Systems n-Octane or Decane + Toluene + Dimethyl Sulfoxide + Methanol or Ethanol at 298.15 K: Experimental Data and Correlation. *J. Solution Chem.* **2018**, *47*, 1127.

(37) Santiago, R. S.; Aznar, M. Quinary liquid−liquid equilibria for mixtures of nonane+undecane+two pairs of aromatics (benzene/toluene/m-xylene)+sulfolane at 298.15 and 313.15K. *Fluid Phase Equilib.* **2007**, *259*, 71−76.

(38) Hizaddin, H. F.; Hadj-Kali, M. K.; Ramalingam, A.; Hashim, M. A. Extraction of nitrogen compounds from diesel fuel using imidazolium- and pyridinium-based ionic liquids: Experiments, COSMO-RS prediction and NRTL correlation. *Fluid Phase Equilib.* **2015**, *405*, 55−67.

(39) Machado, A. B.; Ardila, Y. C.; de Oliveira, L. H.; Aznar, M.; Wolf Maciel, M. R. Liquid−Liquid Equilibrium Study in Ternary Castor Oil Biodiesel + Ethanol + Glycerol and Quaternary Castor Oil Biodiesel + Ethanol + Glycerol + NaOH Systems at (298.2 and 333.2) K. *J. Chem. Eng. Data* **2011**, *56*, 2196−2201.

(40) Wazeer, I.; AlNashef, I. M.; Al-Zahrani, A. A.; Hadj-Kali, M. K. The subtle but substantial distinction between ammonium-and phosphonium-based deep eutectic solvents. *J. Mol. Liq.* **2021**, No. 115838.

(41) Ali, M. C.; Yang, Q.; Fine, A. A.; Jin, W.; Zhang, Z.; Xing, H.; Ren, Q. Efficient removal of both basic and non-basic nitrogen compounds from fuels by deep eutectic solvents. *Green Chem.* **2016**, *18*, 157−164.

(42) Lemaoui, T.; Benguerba, Y.; Darwish, A. S.; Hatab, F. A.; Warrag, S. E. E.; Kroon, M. C.; Alnashef, I. M. Simultaneous dearomatization, desulfurization, and denitrogenation of diesel fuels using acidic deep eutectic solvents as extractive agents: A parametric study. *Sep. Purif. Technol.* **2021**, *256*, No. 117861.

(43) Zhang, H. Liquid−Liquid Phase Equilibria for Quinary, Quaternary, and Ternary Systems {Water + Furfural + Acetic Acid + Cyclopentyl Methyl Ether + CaCl2}: Measurement, Effect of Salt,and Comparative Study. *J. Chem. Eng. Data* **2018**, *63*, 3338−3344.